1B.2 STORM SCALE METEOROLOGICAL PROCESSES IN THE 30 JUNE 2014 DOUBLE DERECHO EVENT

Eric Lenning*, Richard Castro, and Matthew T. Friedlein
NOAA/NWS Chicago, IL

Anthony W. Lyza and Kevin R. Knupp
Severe Weather Institute and Radar & Lightning Laboratories (SWIRLL)
University of Alabama in Huntsville

1. INTRODUCTION

Two quasi-linear convective systems (QLCSs) crossed northern Illinois during the evening hours of 30 June 2014. The first QLCS manifested as a progressive derecho (Johns and Hirt 1987), with numerous high-end wind damage reports across Iowa and northern Illinois. As this began to weaken, a second QLCS formed over central and eastern Iowa. This also exhibited derecho characteristics as it propagated quickly across northern Illinois and northern Indiana before weakening in northwestern Ohio.

While the development of a secondary QLCS certainly is not unusual, the second QLCS in this event was particularly damaging. It generated numerous reports of 35-45 m s^{-1} (80-100 MPH) estimated straight-line wind gusts and at least 29 tornadoes, all rated EF0-EF1. The passage of the second QLCS through a relatively dense surface observational network and good radar coverage allowed for several noteworthy observations. These observations include:

- The bore-driven nature of the second QLCS for its entire lifecycle, as seen from numerous surface observations and a system motion substantially faster than its cold pool or mean tropospheric flow would support;
- A remarkable view of two mesovortices interacting and producing a tornado within 40 km of a terminal Doppler radar and within 10 km of the Chicago-Romeoville NEXRAD radar (KLOT), which detected a maximum wind speed near 66 m s^{-1} (128 kt or 147 MPH) at an elevation of 230-235 m (755-775 ft) AGL;
- Apparent wave interactions with the QLCS, including one associated with mesovortex genesis and formation of an EF1 tornado; and
- Growth and intensification of a mesovortex upon interacting with a remnant thermal boundary from the first QLCS. This mesovortex veered to propagate along the boundary, eventually split into two subvortices, and produced a remarkable flurry of at least 14 confirmed tornadoes, along with widespread damage from winds estimated at 45-50 m s^{-1} (100-110 MPH).

A detailed examination of all four observations is beyond the scope of this presentation. Instead, the focus will be on the first two observations and how mesoscale and especially storm-scale interactions contributed to the severity and tornadic nature of the second QLCS. The presentation also discusses how these observations raise additional questions to be addressed through further research into this case and others.

2. MESOSCALE EVOLUTION AFTER FIRST QLCS

Friedlein et al. (2015) in paper 1B.1 provides a complete overview of the 30 June 2014 event, including a map of the tornado tracks, and describes how the synoptic and mesoscale environment evolved from the first to the second QLCS. One important remnant from the first QLCS was an outflow boundary that stalled south of Lake Michigan between the Kankakee IL (KIKK) and Rensselaer IN (KRZL) observing sites (Figure 1). This boundary took on the characteristics of a warm front as southeasterly winds slowly lifted it back north. At 0200 UTC, prior to the arrival of the second QLCS, KIKK reported a temperature of 21°C (70°F) and dewpoint of 20°C (68°F) in the cold pool north of the boundary. South of the boundary, roughly 60 km away at KRZL, the temperature was 26°C (79°F) and dewpoint was 25°C (77°F).

This boundary later became the focus for tornadic development in the second QLCS but other mesoscale factors such as increasingly favorable storm relative helicity and deep layer shear also aided in mesovortex and tornado production as described in studies such as Thompson et al. (2007) and Thompson et al. (2012). The SPC Mesoscale Analysis website (Hart et al. 2015)

* *Corresponding author address:* Eric Lenning, NOAA/NWS Chicago; 333 W. University Dr., Romeoville, IL 60446; e-mail: Eric.Lenning@noaa.gov

tracked the evolution of these parameters during the event. Based on this mesoanalysis, shear in the 0-6 km layer during the first QLCS was estimated at 20-25 m s^{-1} (40-50 kts, Figure 2a). This was sufficient for supporting organized convection, but weaker than the 25-30 m s^{-1} (50-60 kts) of 0-6 km shear during the passage of the second QLCS (Figure 2b). The SPC mesoanalysis also showed effective storm relative helicity increasing markedly from around 200 m^2 s^{-2} during the first QLCS to a range of 300-700 m^2 s^{-2}, and likely higher, during the second QLCS (Figure 3).

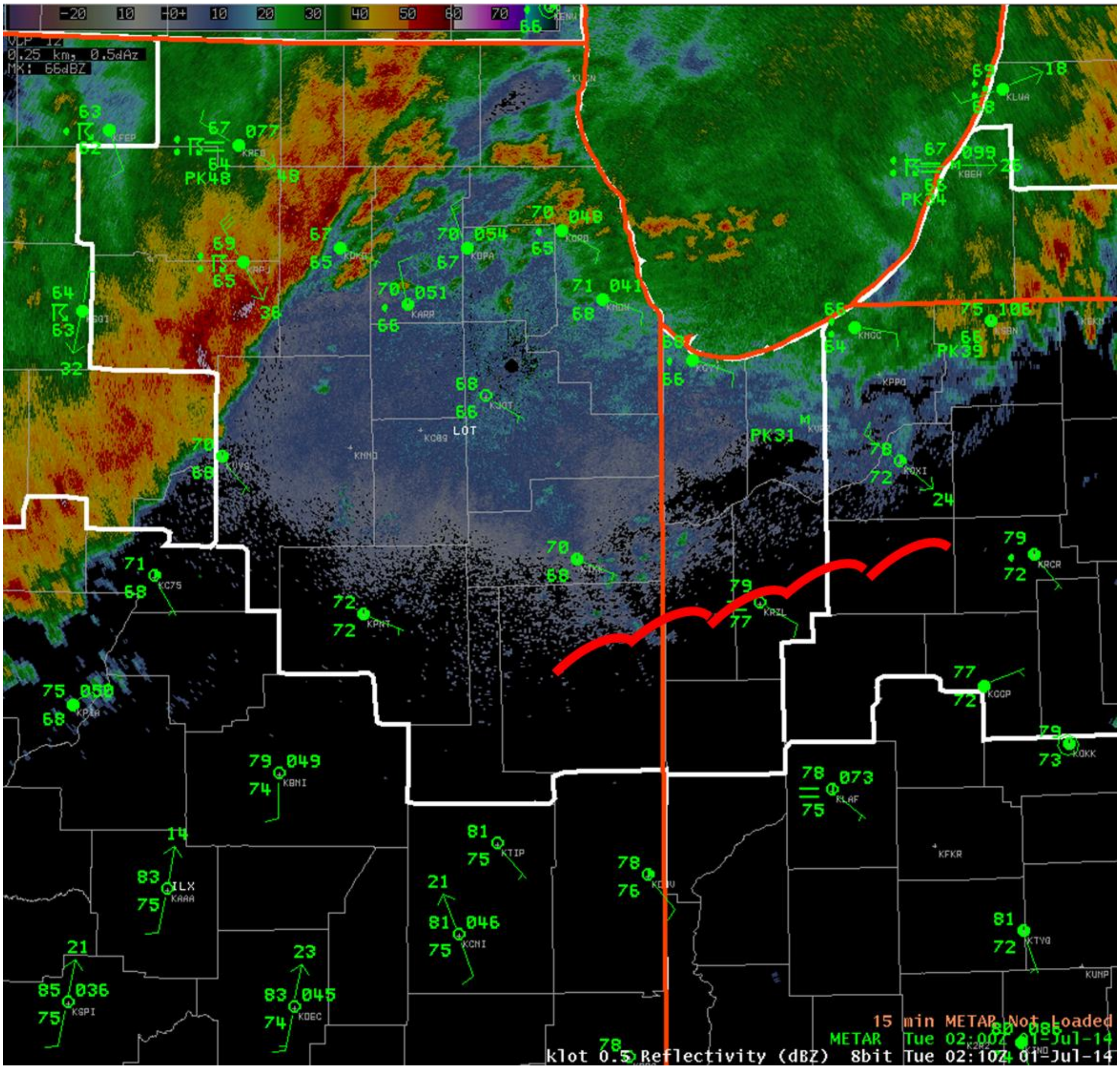

Figure 1. 0200 UTC 1 July 2014 surface observations, KLOT radar reflectivity, and position of remnant outflow boundary from first QLCS which acted as a warm front ahead of the second QLCS.

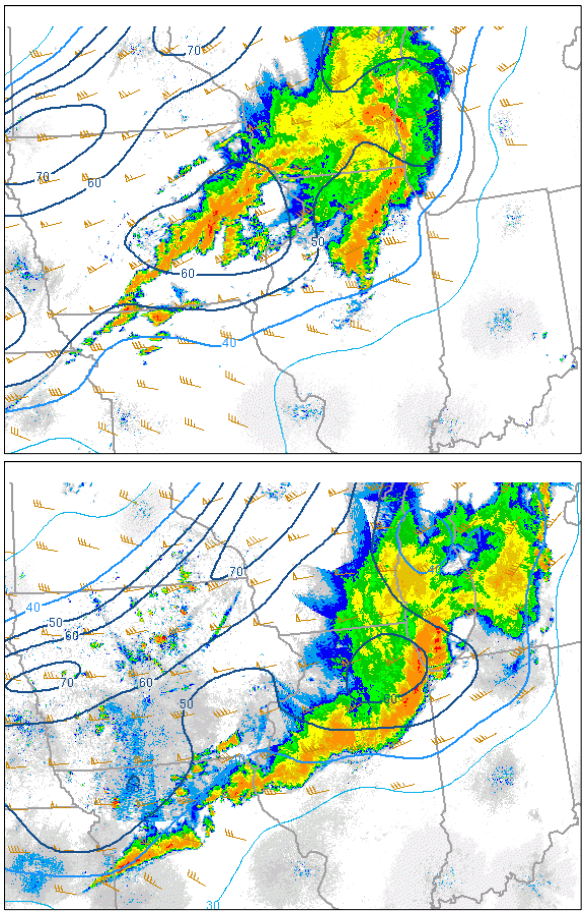

Figure 2. Estimated 0-6 km shear (kts) at (a, top) 2300 UTC 30 June 2014 and (b, bottom) 0300 UTC 1 July 2014.

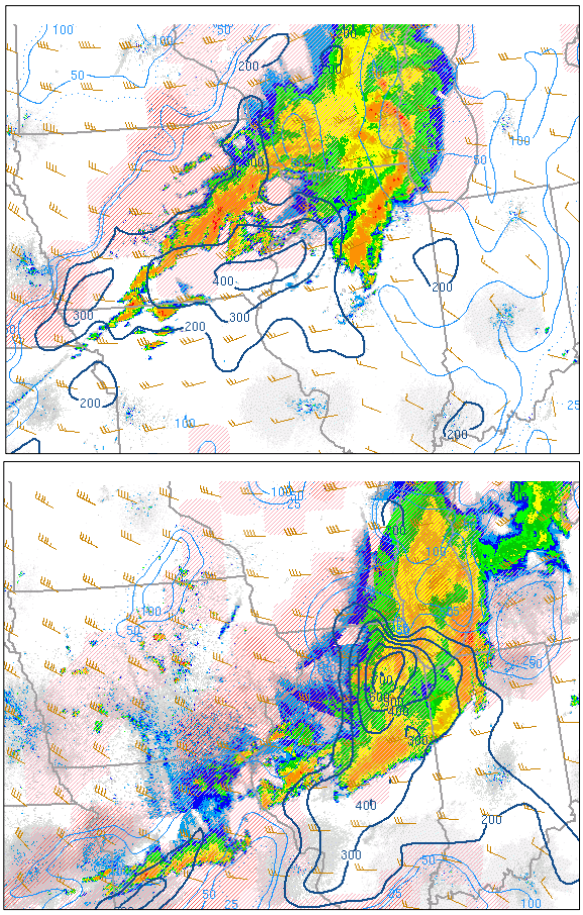

Figure 3. Estimated effective SRH (m^2 s^{-2}) at (a, top) 2300 UTC 30 June 2014 and (b, bottom) 0400 UTC 1 July 2014.

3. MOTION OF THE SECOND QLCS

Despite the increasingly favorable tornadic environment developing ahead of the second QLCS, it appeared possible in real-time operations that the remnant cold pool from the first event would inhibit additional severe weather by keeping the second line of storms elevated above the stable surface layer. In reality, after considering the speed and motion of the second QLCS, it is likely the shallow stable layer played a key role in helping the second line become prolifically tornadic.

The overall motion of the second QLCS was estimated to be east-southeast (103°) at 23 m s^{-1}, though the portion of the QLCS that became tornadic was moving at 26 ms^{-1} and more southeasterly (113°). At the same time, the mean environmental wind was toward the northeast at approximately 20 m s^{-1}. The nearly perpendicular derecho motion relative to the mean wind closely matches the Johns and Hirt (1987) paradigm of a serial derecho rather than a progressive derecho (Figure 4). An upstream cold front and the previously described warm front provide additional support for this idea. However, a serial derecho typically is associated with storm motions under 15 m s^{-1} rather than the 23-26 m s^{-1} estimated during this event.

A time series of observations from the Valparaiso IN (KVPZ) ASOS as the two derechoes passed through early on 1 July 2014 (Figure 5) helps explain what likely was driving the unusual motion in the second line. The first snapshot at 0116 UTC shows the temperature and dewpoint falling rapidly as pressure rises rapidly. The second snapshot at 0340 UTC also shows a pressure rise but at this time the temperature is rising as well. A third snapshot from 0359-0402 UTC shows a slight pressure decrease followed by a sharp jump in pressure, while the temperature continues to rise.

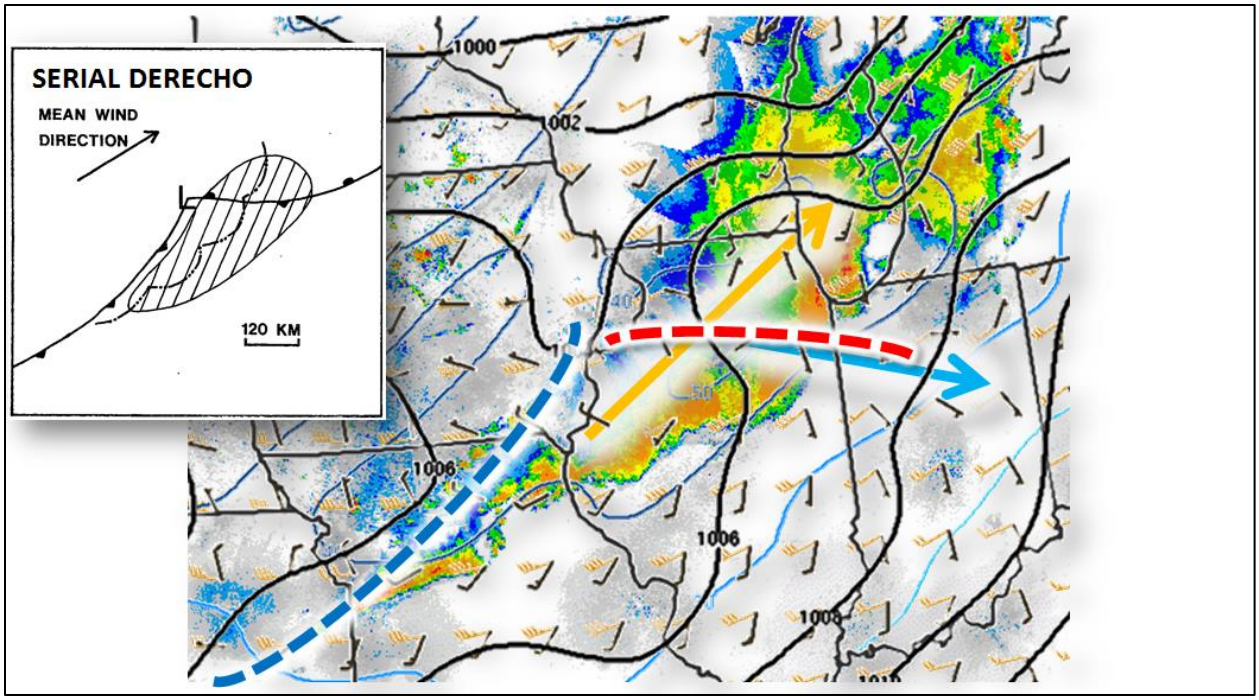

Figure 4. MSLP (mb, black contours), surface winds (kts, black barbs), 850-300mb mean wind (kts, orange barbs), mean wind direction (orange arrow), storm direction of second QLCS (blue arrow), and location of the warm front (red dashed line) and cold front (blue dashed line) at 0300 UTC 1 July 2014.

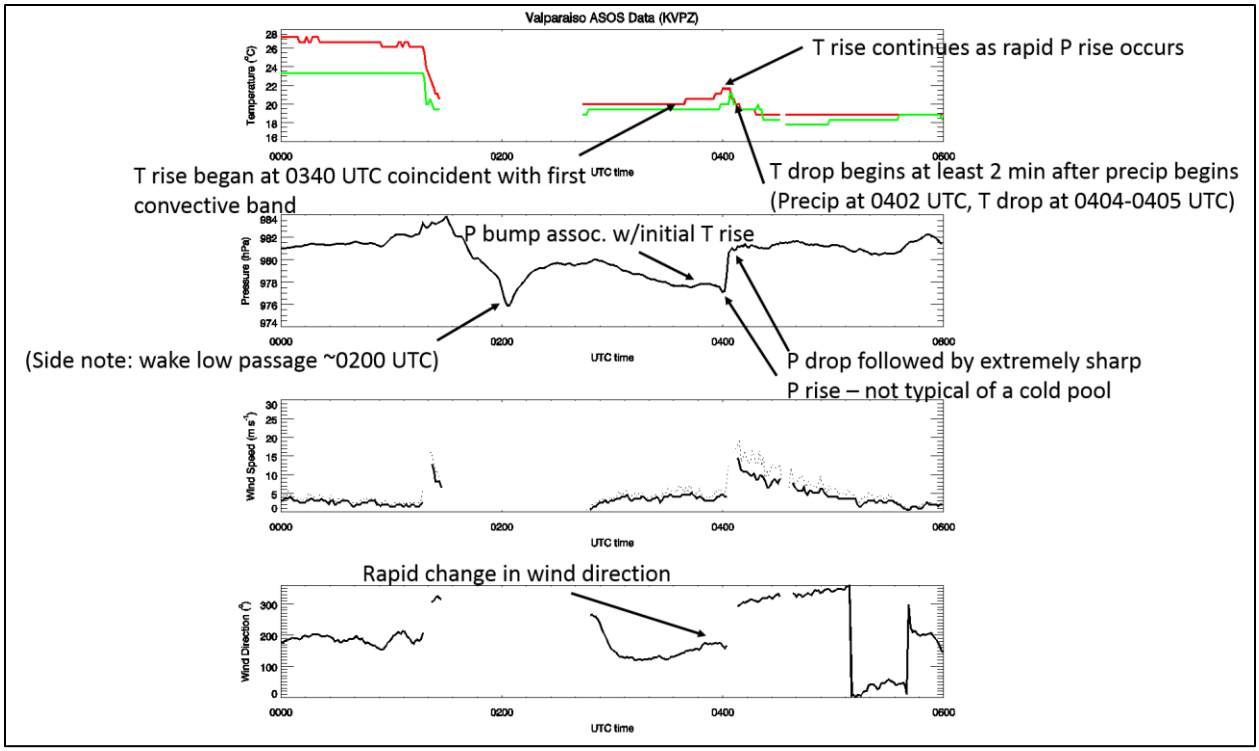

Figure 5. Time series of observations at Valparaiso IN (KVPZ) on 1 July 2014.

A jump in pressure with a drop in temperature and dewpoint is characteristic of a gust front passage, and in this case was coincident with the arrival of the first derecho and the mesohigh within its cold pool. A rise in pressure with a steady or rising temperature, as seen in the second and third snapshots, is more characteristic of the passage of a bore, and in this event occurred just ahead of the second derecho.

4. BORE-DRIVEN NATURE OF THE SECOND QLCS

The likely presence of a bore in this event helps explain why the stable surface layer not only did not inhibit severe weather in the second line but likely contributed to its tornadic severity. A bore, which depends on the presence of a stable boundary layer, has been shown to help destabilize that layer by raising the inversion height and steepening the low level lapse rate (Markowski and Richardson 2010, hereafter MR2010). As such, convection that develops in association with a bore also tends to exhibit much faster motion than convection driven by a density current or cold-pool outflow boundary. This is especially true for an event like 30 June 2014 when the density current is moving through another pre-existing cold pool.

The speed of a density current is related to the contrast in airmass densities across the gust front boundary, while the speed of a bore is related to the contrast in virtual temperatures within and above the stable surface layer. The speed of a density current can be estimated by using the following equation:

$$c = k\sqrt{gH\frac{\rho_1 - \rho_2}{\rho_1}} \qquad (1)$$

where k is a Froude number ranging from 0.7 to 1.3; c is the predicted density current speed; g is the gravitational constant; H is the depth of the density current; and ρ_1 and ρ_2 are the densities of air ahead of and within the density current, respectively (MR2010). The theoretical speed of a bore can be calculated using the following equations:

$$c_{gw} = \left[g\left(\frac{\Delta\theta_v}{\theta_v}\right)h_0\right]^{\frac{1}{2}} \qquad (2)$$

$$c_{bore} = c_{gw}\left[\frac{1}{2}\frac{h_1}{h_0}\left(1 + \frac{h_1}{h_0}\right)\right]^{\frac{1}{2}} \qquad (3)$$

where C_{gw} and C_{bore} are the speeds of an internal gravity wave in a fluid layer and a bore, respectively; θ_v is the virtual potential temperature; and h_0 and h_1 are the depths of the stable fluid layer before and after bore passage, respectively (Coleman et al. 2009). In an operational environment without specialized observations, only approximate values can be obtained for these parameters. However, these approximations still can shed light on the processes that are occurring during an event.

On the evening of 30 June 2014, the actual speed of the first QLCS was estimated at 17 m s^{-1}. This falls within the theoretical cold pool speed of 16-30 m s^{-1} that was calculated for this first QLCS. Calculation of a theoretical bore speed was not possible for the first QLCS since there was not yet a stable layer. In contrast, as previously mentioned, the actual speed of the second QLCS was between 23-26 m s^{-1}. The theoretical cold pool speed for this second QLCS was calculated as 9-17 m s^{-1}. Again, since the second cool pool is moving through the first one, this is slower than the first QLCS due to the smaller density difference between the two cold pools than between the first cold pool and the ambient environment. The theoretical bore speed for the second QLCS was calculated as 26 m s^{-1}, which closely matched the observed speed. Table 1 summarizes these results.

	1st QLCS	2nd QLCS
Actual Speed	17	25
Theoretical Cold Pool Speed	16-30	9-17
Theoretical Bore Speed	n/a	26

Table 1. Actual and theoretical system speeds (m s^{-1}).

Additional evidence for the presence of a bore on 30 June 2014 is provided by traces of temperature, dewpoint, and pressure observed at six additional locations along the path of the second QLCS (Figure 6). At each station, at least until deep moist convection began to dominate the signal, a sharp rise in pressure was accompanied by rising or steady temperatures when the bore moved through.

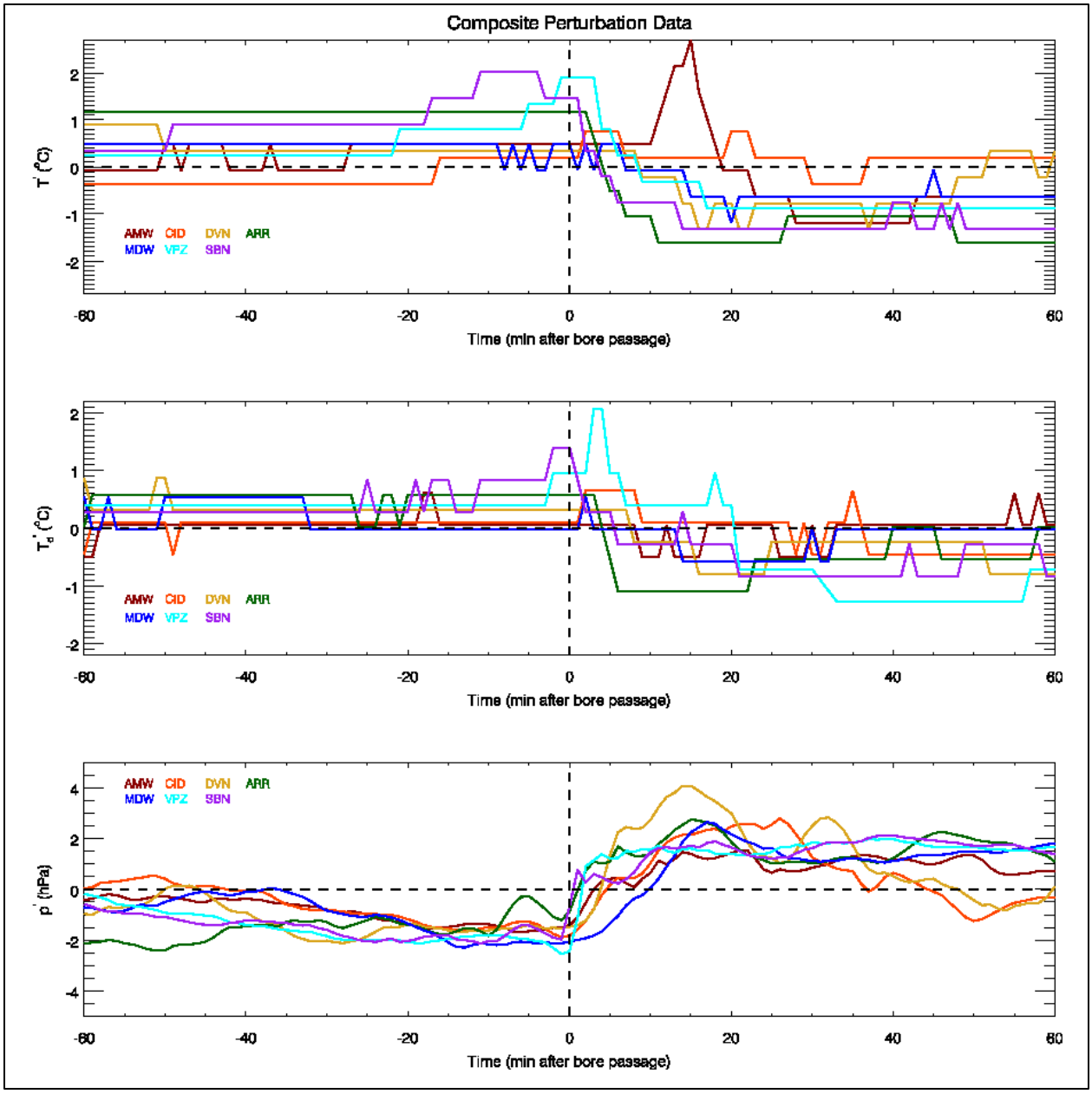

Figure 6. Temperature, dewpoint, and pressure perturbations at seven ASOS locations along path of second QLCS.

5. BORE-DRIVEN ENHANCEMENT OF STORM RELATIVE HELICITY

As previously mentioned, the magnitude of storm relative helicity in the lowest levels of the atmosphere has been shown to be correlated with the likelihood that storms will produce tornadoes. These SRH values depend both on environmental winds as well as the motion of the storms. In a typical severe weather environment where winds increase and veer with height, a faster and more southeasterly storm motion will tend to increase SRH values. Figure 7 shows calculations of SRH using environmental winds estimated from the Extended Velocity Azimuth Display (EVAD, Matejka and Srivastava, 1991) at KLOT and three different storm motions.

On the evening of 30 June into 1 July 2014, the SPC mesoanalysis showed effective SRH values ahead of the second QLCS to be considerably larger than with the first QLCS. Furthermore, SPC calculates these values relative to the estimated speed and direction of a right-moving supercell which at the time of interest was around 17 m s^{-1} to the east (Figure 7. Hodographs using EVAD winds from KLOT showing changes in 0-1km

SRH (red shading) and 0-3 km SRH (red and purple shading) calculated from three different storm motions at 0249 UTC 1 July 2014.. Thus the true storm motion further increased the environmental SRH, bringing it to extreme levels for the second QLCS (Figure 7, lower right). Figure 8 shows the computed values for 0-1 km and 0-3 km SRH based on EVAD winds from KLOT and how these values changed over time.

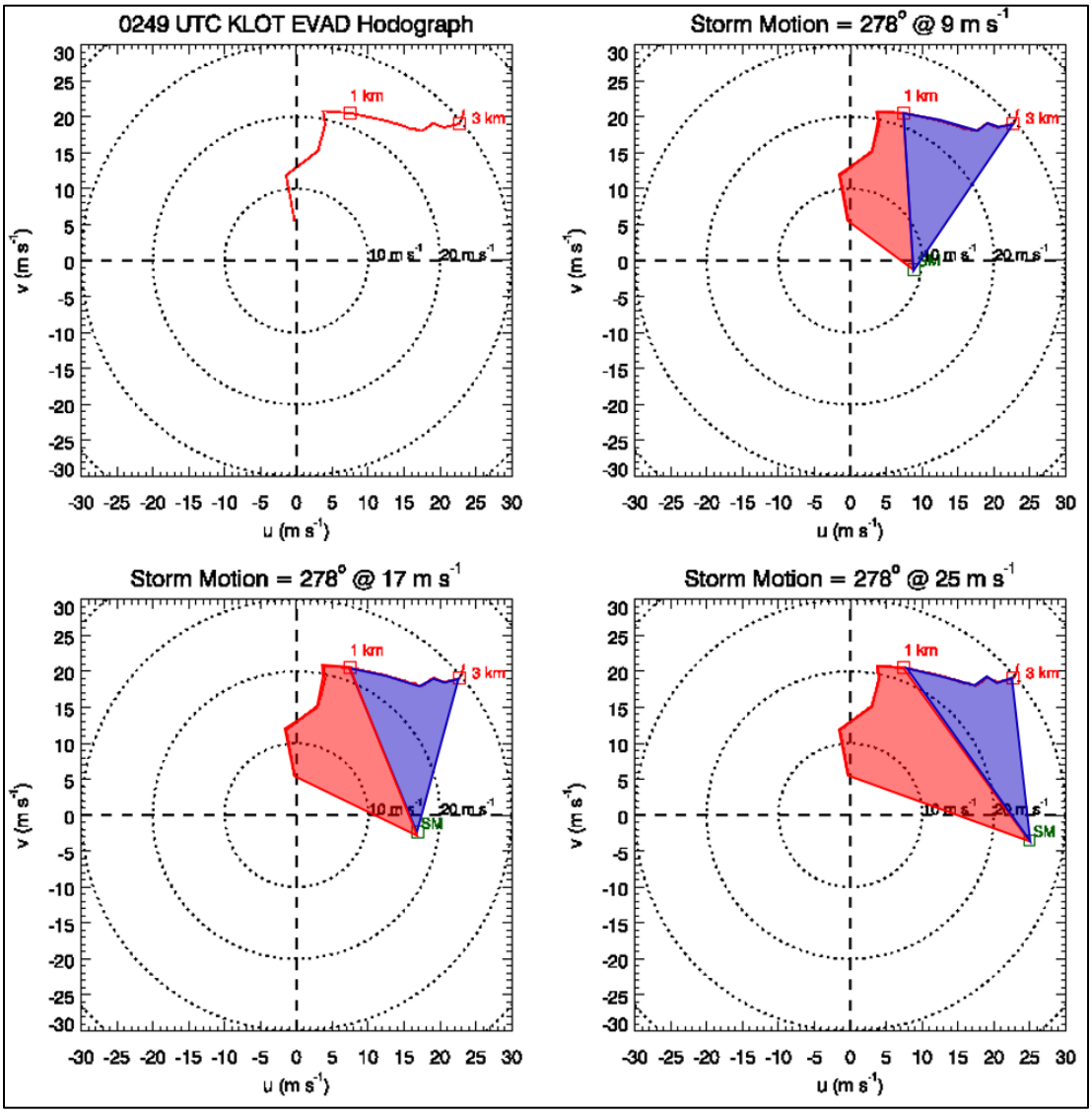

Figure 7. Hodographs using EVAD winds from KLOT showing changes in 0-1km SRH (red shading) and 0-3 km SRH (red and purple shading) calculated from three different storm motions at 0249 UTC 1 July 2014.

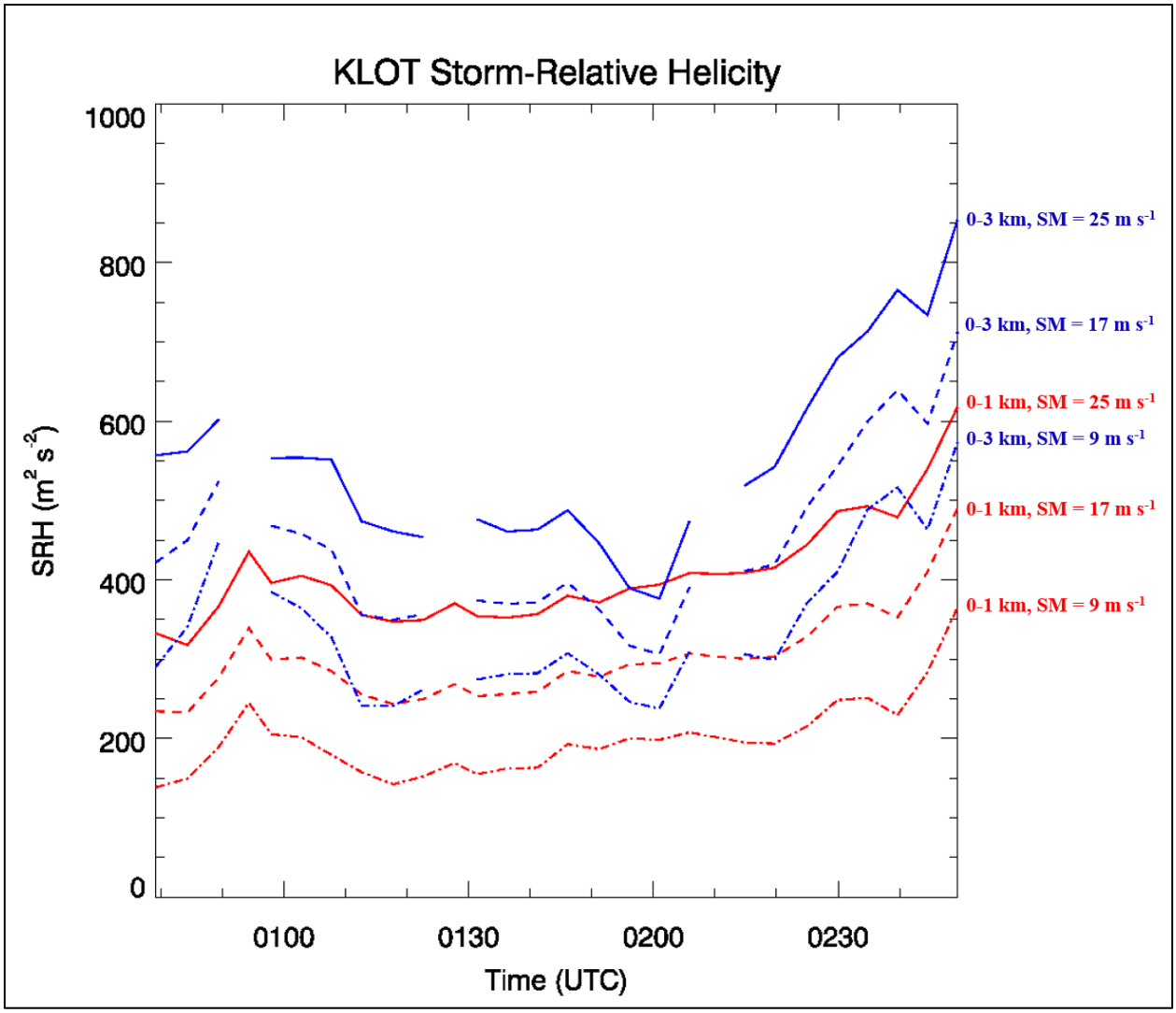

Figure 8. Evolution of 0-1 km (red) and 0-3 km (blue) SRH based on EVAD winds at KLOT for three different storm motions on 1 July 2014.

In summary, the bore-driven nature of the second QLCS influenced the severity of this line in multiple ways:

- It allowed the second QLCS to ingest surface or near-surface parcels within the remnant cold pool, rather than riding over this stable layer, and also helped destabilize this layer;
- It assisted in lifting surface or near-surface parcels to the top of the stable layer; and,
- It provided for a faster storm propagation which enhanced SRH values to extreme levels.

This combination of factors prior to arrival of the second QLCS led to an environment highly supportive of tornadic activity, including the potential for strong and violent tornadoes.

6. RADAR SIGNATURES IN THE SECOND QLCS

As previously stated, the most notable aspect of the event on 30 June 2014 was not the rapid succession of two intense derechoes, but the prolific generation of tornadoes over a relatively small time and space scale by the second one. Additionally, despite the extreme values of SRH, no tornado was rated stronger than high-end EF1 although the lack of damage indicators in the affected area likely played some role in this. This suggests that the tornadic potential of the environment was realized in quantity rather than magnitude.

When the atmosphere is supportive of mesovortices in close proximity, interactions between these circulations also can occur. These interactions often are too distant or shallow for detection by fixed

radars, though on 30 June 2014 two mesovortices developed less than 10 km to the west of KLOT and less than 40 km from the Midway terminal Doppler radar (TMDW). These vortices ended up producing a tornado, thus offering an opportunity to witness the interaction of two mesovortices during the process of tornadogenesis (Figure 9).

The motion of these two circulations generally matched what would be expected of two vortices of like sign in close proximity based on the work of Fujiwhara (1931, Figure 10). In this case the circulations were of similar strength, with the northern one possibly a bit stronger. This led to the two vortices rotating around each other with the southern one pushing a little faster to the east around the northern one.

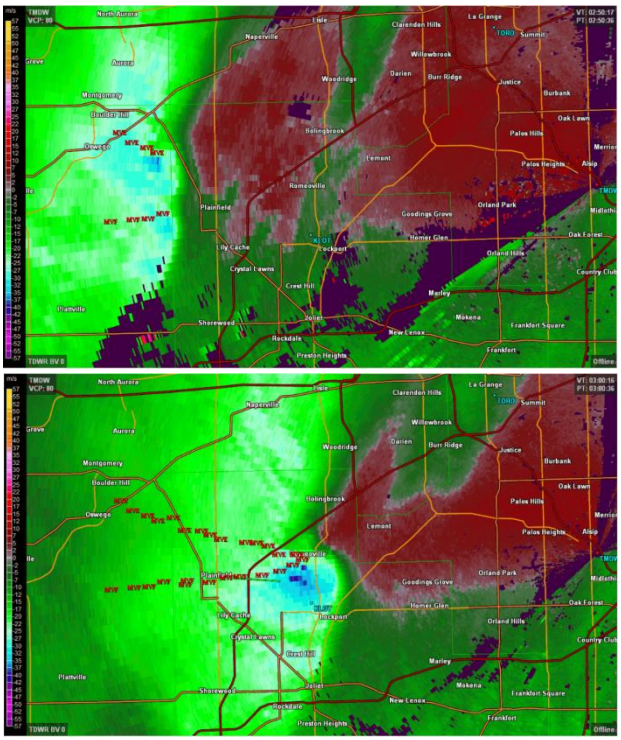

Figure 9. TMDW base velocity at 0250 UTC (top) and 0300 UTC (bottom) on 1 July 2014 at the 0.5 degree radar elevation. Circulation centroid paths are shown by the red “MVF” labels.

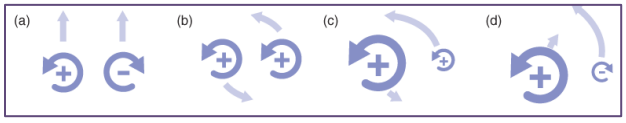

Figure 10. Idealized Fujiwhara interactions between two point vortices. From MR2010.

The ability to examine this process at one location sheds light on what may have been happening elsewhere on this evening and during previous events where damage surveys have revealed the presence of multiple tornado tracks in close proximity (e.g. Forbes and Wakimoto, 1983, and Przybylinski, 2002 and 2004). These radar images support the idea that multiple circulations in close proximity can produce parallel damage paths, convergent or divergent paths, and even merging or crossing paths.

7. SUMMARY AND DISCUSSION

This presentation has reviewed radar and surface observations on the evening of 30 June 2014 and discussed the role of mesoscale and storm-scale interactions that contributed to the severity and tornadic nature of the second QLCS during this event. The bore-driven nature of the second QLCS was key in tying this feature to the surface layer, destabilizing this layer, and greatly enhancing values of SRH. Within this QLCS, two circulations developed in close proximity to each other and within 40 km of the TMDW radar and 10 km of the KLOT radar. The interaction of these circulations demonstrated one way tornadoes can form and behave in such an environment.

The event on 30 June 2014 also raises numerous questions for further study, including:

- How does mesovortex formation differ between a bore-driven and cold-pool driven QLCS?
- How common is a bore-driven QLCS?
- Does a bore-driven QLCS increase or intensify the risk of severe weather?
- What is the process of tornadogenesis in large mesovortices? What is the source of surface vorticity?
- Does the paradigm of highest tornado intensity being near the surface apply to QLCS tornadoes? How common is that intensity profile overall?

Beyond these questions, there is also the challenge of recognizing the presence and influence of a bore during real-time forecast and warning operations. If additional studies reveal the bore-driven QLCS process to be more common than presently understood, it could become necessary to develop new techniques for analyzing surface observations. These techniques would require access to 1-minute ASOS data and an automated method for interrogating these data to discern the presence of relevant trends.

8. REFERENCES

Coleman, T. A., K. R. Knupp, and D. Herzmann, 2009: The Spectacular Undular Bore in Iowa on 2 October 2007. *Mon. Wea. Rev.*, **137**, 495–503.

Forbes, G.S., and R. M. Wakimoto, 1983: A Concentrated Outbreak of Tornadoes, Downbursts and Microbursts, and Implications Regarding Vortex Classification. *Mon. Wea. Rev.*, **111**, 220–236.

Friedlein, M. T., E. Lenning, R. Castro, A. W. Lyza, and K. R. Knupp, 2015: Evolution of the 30 June 2014 Double Derecho Event in Northern Illinois & Northwest Indiana. *27st Conf. on Weather Analysis and Forecasting,* Chicago, IL, Amer. Meteor. Soc., 1B.1. [Available online: https://ams.confex.com/ams/27WAF23NWP/webprogram/Paper273796.html]

Fujiwhara, S., 1931: Short note on the behavior of two vortices. *Proc. Phys.-Math. Soc. Japan*, **13**, 106-110.

Hart, J., C. Mead, P Bothwell, and R. Thompson/ Storm Prediction Center, 2015: SPC Mesoscale Analysis Pages. Accessed 6 August 2015. [Available online at http://www.spce.noaa.gov/exper/mesoanalysis/]

Johns, R. H., and W. D. Hirt, 1987: Derechos: Widespread Convectively Induced Windstorms. *Wea. Forecasting*, **2**, 32–49.

Markowski, P. M., and Y. P. Richardson, 2010: *Mesoscale Meteorology in Midlatitudes*, Wiley-Blackwell, 407 pp.

Matejka, T., and R. C. Srivastava, 1991: An Improved Version of the Extended Velocity-Azimuth Display Analysis of Single-Doppler Radar Data. *J. Atmos. Oceanic Technol.*, **8**, 453–466.

Przybylinski, R. P., 2002: May 1st, 2002 Severe Weather Event - Tornadoes across Bond and Marion Counties, Illinois. Accessed 6 August 2015. [Available online at http://www.weather.gov/lsx/05_01_2002]

_____, 2004: May 30th, 2004, Severe Weather Outbreak. Accessed 6 August 2015. [Available online at http://www.weather.gov/lsx/05_30_2004]

Thompson, R. L., C. M. Mead, and R. Edwards, 2007: Effective Storm-Relative Helicity and Bulk Shear in Supercell Thunderstorm Environments. *Wea. Forecasting*, **22**, 102–115.

_____, B. T. Smith, J. S. Grams, A. R. Dean, and C. Broyles, 2012: Convective Modes for Significant Severe Thunderstorms in the Contiguous United States. Part II: Supercell and QLCS Tornado Environments. *Wea. Forecasting*, **27**, 1136–1154.